Nonthermal Site Occupation at the Donor-Acceptor Interface of Organic Solar Cells

A. N. Brigeman, M. A. Fusella, B. P. Rand, and N. C. Giebink

Phys. Rev. Applied **10**, 034034 — Published 18 September 2018

DOI: 10.1103/PhysRevApplied.10.034034

Non-thermal site occupation at the donor-acceptor interface of organic solar cells

A. N. Brigeman,[1] M. A. Fusella,[2] B. P. Rand,[2,3] and N. C. Giebink[1,*]

[1]*Department of Electrical Engineering, The Pennsylvania State University, University Park, Pennsylvania 16802, USA*

[2]*Department of Electrical Engineering, Princeton University, Princeton, New Jersey 08544, USA*

[3]*Andlinger Center for Energy and the Environment, Department of Electrical Engineering, Princeton University, Princeton, New Jersey 08544, USA*

[*]ncg2@psu.edu

Abstract

We explore the nature of occupation and relaxation within the charge transfer density of states (CT DOS) for bulk heterojunction organic solar cells consisting of the donor boron subphthalocyanine chloride and the acceptor C_{60}. We observe relaxation of geminate CT states on a sub-ns timescale via a ~70 meV dynamic redshift in their photoluminescence, whereas free carrier relaxation at longer times leads to the formation of non-geminate CT states at even lower energy. In steady-state, we find that thermalization within the DOS is incomplete, resulting in a Boltzmann-like CT state distribution characterized by an effective temperature above that of the ambient. These results confirm that electron and hole populations can be far from equilibrium in organic solar cells and may prompt a reassessment of analyses that assume the same temperature for their charge carrier distributions in the dark and under illumination.

I. INTRODUCTION

The efficiency of organic photovoltaic (OPV) cells is governed by a balance between charge separation and recombination at the donor-acceptor (DA) interface, mediated by charge transfer (CT) states that consist of a donor hole Coulombically bound to a neighboring acceptor electron [1,2]. Previous work has established a clear link between the efficiency of a given OPV cell and the properties of its CT state such as, for example, the relationship between open-circuit voltage (V_{OC}), CT state energy, and recombination rate, or the impact of CT state delocalization on short-circuit current (J_{SC}) [3-6]. These conclusions are made, however, with the tacit understanding that there is not one CT state, but rather a distribution, that is, a CT density of states (DOS) due to the positional, rotational, and conformational disorder of nearby D and A molecules, aggregates, and crystallites [6-10]. Yet, despite the implications that such a distribution introduces (such as added voltage loss [6,8,10,11] and the potential for barrier-less charge separation [12-14]), surprisingly little is known about the form of the CT state DOS, how CT states relax within it, and how the CT DOS relates to the joint density of free electron and hole states.

Perhaps most importantly, the question of whether the CT DOS is occupied in equilibrium fashion has come under scrutiny. Most device modeling to date assumes quasi-equilibrium Fermi-Dirac statistics in determining carrier concentrations and thus CT state occupation at the DA interface [15,16]. However, recent work has called this into question, suggesting that occupation of the free carrier DOS is in fact far from equilibrium and that electrons and holes are extracted before they fully thermalize [17-19]. This claim, which is based on strongly dispersive transport of photogenerated electrons and holes observed in transient mobility experiments, has

not gone unchallenged [20], leading to an ongoing debate over the relevance of nonequilibrium site occupation in disordered OPV cells.

Here, we present direct spectroscopic evidence of non-thermal occupation in the CT DOS of small molecule OPV cells involving the donor boron subphthalocyanine chloride (SubPc) and acceptor C_{60}. We observe a sub-ns dynamic redshift in the transient CT photoluminescence (PL) that attests to geminate CT state relaxation followed by an even larger redshift on longer timescales due to non-geminate CT states formed from free charges that have relaxed further in the DOS. At steady-state, we find that the CT state PL is characterized by an effective temperature above that of the sample itself, and that this discrepancy becomes more pronounced with decreasing (sample) temperature as hopping transport to the lowest energy DOS sites is increasingly frustrated. This result carries important implications for device modeling and may also prompt a re-evaluation of common V_{OC} and ideality factor analyses that implicitly assume illuminated OPV charge carrier distributions to be at the ambient temperature.

II. METHODS

A. Sample preparation

Solar cells and DA blend film samples are deposited by vacuum thermal evaporation in a chamber with a base pressure of 10^{-7} Torr onto pre-patterned indium-tin-oxide (ITO) glass and fused silica substrates, respectively. The organic source materials boron subphthalocyanine chloride (SubPc), fullerene C_{60}, and bathocuproine (BCP) are all purified via thermal gradient sublimation and are purchased from Sigma Aldrich, SES Research, and Lumtec, respectively. The solar cell device architecure consists of a 100 nm-thick SubPc:C_{60} active layer deposited on an ITO/glass substrate followed by a 10 nm BCP buffer and a 100 nm Al cathode defined by a shadow mask. Bulk heterojunction SubPc:C_{60} devices with a similar structure have previously

been explored in detail and exhibit V_{oc} ~ 1 V with efficiencies ranging from 1.55 - 3.70% depending on the SubPc:C_{60} blend fraction [21]. To avoid glass autofluorescence, PL experiments are carried out on fused silica substrates using the same SubPc:C_{60} (100 nm)/BCP (10 nm)/Al (100 nm) device stack to maintain a similar microcavity environment as complete solar cells.

B. Characterization

Time-resolved PL spectroscopy is carried out using a Hamamatsu C10910 streak camera (~10 ps temporal resolution) synced to an EKSPLA optical parametric oscillator with a ~20 ps pulse width and 1 kHz repetition rate at λ = 532 nm and a pulse fluence of 130 μJ/cm^2. Steady-state PL spectra are excited at the same wavelength using a continuous-wave laser (intensity ~500 mW/cm^2) and collected using a fibre-coupled spectrometer with cooled Si CCD and InGaAs array detectors. Low temperature measurements are carried out in an optically accessible cryostat, with device temperature measured using a Si temperature diode adhered directly to the surface of each sample.

III. RESULTS AND DISCUSSION

Figure 1 illustrates the full range of charge generation and recombination processes in a typical bulk heterojunction (BHJ) organic solar cell operating at open circuit, where each excited state manifold/energy level is inhomogeneously broadened by disorder. Following the initial D→A charge transfer event, the resulting hot CT state may dissociate directly or undergo internal conversion to the lowest CT manifold on a ~ps timescale [22]. At this point, the bound CT state may relax geminately within the CT DOS (process 1, defined as the coupled motion of the e^- and h^+ toward lower energy CT sites) or it may dissociate, producing free carriers that relax independently and recombine non-geminately back into a CT state (process 2). The dispersive

nature of the latter process was originally described for amorphous inorganic semiconductors [23] before its more recent extension to organic systems [24,25]. In all cases, the final result is CT decay to the ground state. The possibility of non-thermal CT DOS occupation arises because the motion of electrons and holes needed to reach the lowest energy CT sites in the DOS tail may be restricted by a combination of slow hopping transport and tortuous transport pathways enforced by the BHJ geometry. If, on average, electrons and holes recombine (as geminate or non-geminate CT states) or are extracted before they can fully relax into the DOS tail, then the resulting steady-state distribution of CT states will be non-thermal.

A. CT state relaxation

Figure 2(a) presents the transient CT PL decay of a 1:1 SubPc:C_{60} blend film. The spectrum displays a clear dynamic redshift in the first nanosecond (see Fig. 2(b)) that is summarized together with 1:2 and 4:1 SubPc:C_{60} blend ratios in Fig. 3(a). This CT PL redshift is similar to that observed previously in other small molecule [26] and polymer [27] DA blends. Interestingly, all of the films complete the same ~70 meV redshift within the first few nanoseconds, but with a much different increase in PL broadening over the same timescale as shown in Fig. 3(b). Among the three films, the fastest redshift correlates with the largest degree of broadening in the 1:1 blend. This may simply reflect the larger density of DA interface sites available in an equally-mixed film [28] that facilitate bound CT state relaxation. Unfortunately, it was not possible to test this hypothesis over a wider range of blend ratios (i.e. more C_{60}-rich or SubPc-rich) due to incomplete quenching of C_{60} or SubPc fluorescence, which obscures the weak CT emission; a comparison of these different spectra is provided in the Supplemental Material [29].

Although the CT PL peak appears to have settled at the end of the ns-scale time window in Fig. 3, the steady-state CT PL spectrum of each film is further redshifted, pointing to additional

relaxation in the intervening μs-ms time range. The difference between early time (0-0.5 ns) and steady-state CT PL is shown for the 1:1 blend film in Fig. 4(a) and 4(b) for a range of different substrate temperatures. In contrast to the early time CT PL, which remains largely unchanged with decreasing temperature, the steady-state spectra exhibit a clear blue-shift. The same general behavior is summarized for all of the blend ratios in Fig. 4(c)-4(e).

Collectively, the data in Figs. 2-4 are consistent with geminate CT state relaxation (process 1 in Fig. 1) occurring on a ns timescale followed by non-geminate relaxation (process 2) on a longer timescale. In addition to the clear separation in redshift dynamics that are consistent with the lifetime of each species (i.e. ns for geminate CT states [6] versus μs-ms for free charge [30,31]), this assignment is supported by the functional form of the CT PL decay in Fig. 5, which is monoexponential at early times (expected for geminate recombination) and transitions to a power law at later times (expected for non-geminate recombination) [30].

Additional support follows from the electric field dependence of the CT PL spectra, where reverse biasing a 1:1 blend OPV device has little effect on the shape of the early time (0-0.5 ns) spectrum in Fig. 6(a) yet leads to a substantial blue-shift of the steady-state PL spectrum in Fig. 6(b). This observation is consistent with the expectation that reverse bias should accelerate the extraction of free charges before they can fully relax, effectively shifting occupation of the DOS toward higher energy as reflected by the relative increase in CT PL intensity on the high energy side of the steady-state spectra. The field dependence of the CT PL intensity n Fig. 6(c) follows similarly. There, quenching of the early time PL saturates in reverse bias at -3 V, reflecting the limit of geminate CT state dissociation, whereas the steady-state PL intensity continues to decrease since it also reflects emission from non-geminate CT states that form at later times (in competition with increasingly efficient free charge extraction).

B. Non-thermal occupation

Given the substantial non-geminate relaxation that takes place between early times and steady-state, it is important to determine whether or not relaxation is complete, that is, whether steady-state CT occupation of the DOS is described by a thermal equilibrium Boltzmann factor $\propto \exp[(\mu_{\mathrm{CT}} - E)/k_{\mathrm{b}}T]$ set by the CT state chemical potential (μ_{CT}) and ambient temperature, T [6]. The answer according to Fig. 4 is no: the separation between early time and steady-state CT PL, which is an exclusive measure of how much the distribution has thermalized (since any intrinsic temperature shift in CT energy or DOS should already be accounted for in the early time spectra [6,33]), trends smaller with decreasing temperature, which is opposite to the expectation of a steepening Boltzmann tail. Instead, these data suggest that relaxation is a thermally-assisted process where carriers must hop through higher energy sites to ultimately reach those with the lowest energy in the DOS tail (which are small in number and far apart by definition). Coupled with the geometric frustration of navigating intricate D or A pathways set by the amorphous BHJ morphology [21] (e.g. as sketched in Fig. 1), it is clear why carriers may increasingly fail to reach the bottom of the DOS before being extracted or recombining.

Although the form of the non-equilibrium CT state distribution is not explicitly known, a reasonable starting point is to assume it is Boltzmann-like, but described by an elevated effective temperature. To explore this possibility, we examine the steady-state CT PL in the context of the generalized Planck equation for semiconductor luminescent radiation derived by Würfel [34]:

$$I(E) = A(E)\frac{2\pi E^2}{h^3c^2}\left[\frac{1}{\exp[(E-\mu_{\mathrm{CT}})/k_{\mathrm{b}}T]-1}\right], \quad (1)$$

where $I(E)$ is the spectral photon flux as a function of energy E, $A(E)$ is the material absorbance, h is Planck's constant, c is the speed of light in vacuum, k_{b} is Boltzmann's constant and T is the luminescence temperature. Equation (1) has been shown to hold for a variety of

inorganic and disordered thin film semiconductors [35-37], and it is the basis for the photovoltaic reciprocity relations that have been widely applied to the analysis of open-circuit voltage in OPV cells [3,38-40]. It is commonly used to determine the temperature of inorganic semiconductors based on their luminescence spectrum [41]; however, applying it to OPV DA material systems is complicated by the challenge of accurately measuring the weak CT absorbance tail [$A(E)$], which typically varies by several orders of magnitude over the spectral range of CT luminescence [33,39]. To circumvent this difficulty, we instead examine the log ratio of CT luminescence spectra obtained at a given sample temperature, T_1, relative to that at another temperature, T_2:

$$\ln\left(\frac{I_{\mathrm{T}_1}}{I_{\mathrm{T}_2}}\right) = \left(\frac{\mu_{\mathrm{CT1}}}{k_{\mathrm{b}}T_1} - \frac{\mu_{\mathrm{CT2}}}{k_{\mathrm{b}}T_2}\right) - \frac{E}{k_{\mathrm{b}}}\left(\frac{1}{T_1} - \frac{1}{T_2}\right). \quad (2)$$

This formulation assumes that the temperature dependence of $A(E)$ can be neglected and invokes the Boltzmann approximation to yield a linear expression whose slope is equal to the reciprocal temperature difference; the validity of both assumptions is detailed in the Supplemental Material [29].

Using Eq. (2), it is therefore possible to compare the CT PL spectra obtained at different substrate temperatures and determine whether the difference in their corresponding luminescence temperatures is consistent. Figure 7(a) plots the PL log ratio of the room temperature spectrum in Fig. 4(b) compared to those at lower temperatures, demonstrating the linear relationship predicted by Eq. (2). In this case, the slope of linear fits to the data (solid lines) should be compared with those of the equivalently-colored dashed lines expected from the measured substrate temperatures. In general, the data slopes are smaller than their dashed line counterparts, indicating that the luminescence temperature exceeds that of the substrate. In similar experiments carried out with a GaAs wafer, the luminescence and substrate temperature

differences are nearly identical. These data, as well as intensity-dependent control experiments to rule out local heating of the organic film by the pump laser, are provided in the Supplemental Material [29].

Figure 7(b) summarizes the results for all blend ratios by plotting their CT luminescence temperature as a function of substrate temperature. In each case, we use the room temperature CT PL spectrum as the reference, assuming that its luminescence temperature is actually $T = 293$ K even though it is in fact probably higher. This plot therefore represents a lower bound on luminescence temperature. As compared to the thermal luminescence of the GaAs sample, the CT PL from all of the DA blends is clearly non-thermal and grows more so with decreasing temperature as inferred from Fig. 4 above. In general, the CT state distribution becomes more thermal with increasing C_{60} fraction, presumably due to the associated increase in charge carrier mobility (roughly three orders of magnitude for electrons and one order of magnitude for holes [21]) that facilitates migration to the lowest energy DOS sites.

Another manifestation of non-thermal CT state occupation is the anomalous redshift of CT electroluminescence (EL) relative to PL commonly observed in the literature [4,42] and shown for the 1:1 SubPc:C_{60} blend at room temperature in Fig. 8(a). In contrast to photoinduced charge transfer that uniformly populates the CT DOS, electrical excitation fills the DOS in a relaxed fashion from the bottom up according to the local quasi-Fermi level splitting, with any temperature increase beyond ambient due to Joule heating. The CT EL spectrum is therefore expected to more closely reflect a thermalized CT distribution and should provide a reasonable reference from which to calibrate the absolute PL temperature via Eq. (2). Figure 8(c) shows that the PL-to-EL log ratio for the 1:1 SubPc:C_{60} device does indeed result in a straight line which, in contrast to the GaAs solar cell data shown for reference (see Fig. 8(b)), yields an elevated

effective PL temperature of $T_{\mathrm{eff}} = 330 \pm 3$ K characterizing the CT state distribution under illumination. In this context, it is important to note that the SubPc:C_{60} blend is uniformly mixed and amorphous as established by Pandey et al. [21], unlike phase-separated polymer DA systems where it has been suggested that CT PL and EL originate from distinct regions of the blend film [42].

IV. CONCLUSION

In summary, we have shown that photogenerated CT states in a SubPc:C_{60} BHJ relax geminately by ~70 meV on a ns timescale and that free carriers relax on longer timescales to form non-geminate CT states even lower in the DOS. These relaxation processes occur via thermally-assisted hopping and are generally insufficient to establish a thermal equilibrium distribution of CT states at room temperature. Based on similar observations for other small molecule DA blends (provided in the Supplemental Material [29]**Error! Reference source not found.**) and the hallmark CT PL to EL redshift observed in many polymer DA systems [4,42], non-thermal occupation of the CT DOS (and by extension the free carrier DOS since free carriers and CT states are believed to be in equilibrium with one another [6,16]) is likely to be a general phenomenon in BHJ OPV cells. Beyond the performance implications discussed previously [17-19], non-thermal DOS occupation may force a re-evaluation of trends in V_{OC} (such as, e.g. the slope of V_{OC} versus temperature [33] or the ideality factor deduced from its intensity dependence [43]) that implicitly assume charge carriers to be at the ambient cell temperature.

Acknowledgements

The authors thank Alex Grede for assistance with measuring GaAs reference samples.

References

[1] T. M. Clarke and J. R. Durrant, Charge photogeneration in organic solar cells, Chem. Rev. **110**, 6736 (2010).

[2] C. Deibel, T. Strobel, and V. Dyakonov, Role of the charge transfer state in organic donor–acceptor solar cells, Adv. Mater. **22**, 4097 (2010).

[3] K. Vandewal, K. Tvingstedt, J. V. Manca, and O. Inganäs, Charge-transfer states and upper limit of the open-circuit voltage in polymer:fullerene organic solar cells, IEEE J. Quant. Electron **16**, 1676 (2010).

[4] B. Bernardo, D. Cheyns, B. Verreet, R. D. Schaller, B. P. Rand, and N. C. Giebink, Delocalization and dielectric screening of charge transfer states in organic photovoltaic cells, Nat. Comm. **5**, 3245 (2014).

[5] S. Gélinas, A. Rao, A. Kumar, S. L. Smith, A. W. Chin, J. Clark, T. S. Van der Poll, G. C. Bazan, and R. H. Friend, Ultrafast long-range charge separation in organic semiconductor photovoltaic diodes, Science **343**, 512 (2014).

[6] T. M. Burke, S. Sweetnam, K. Vandewal, and M. D. McGehee, Beyond Langevin recombination: how equilibrium between free carriers and charge transfer states determines the open-circuit voltage of organic solar cells, Adv. Energy Mater. **5**, 1500123 (2015).

[7] R. A. Street, Electronic structure and properties of organic bulk-heterojunction interfaces, Adv. Mater. **28**, 3814 (2016).

[8] J. C. Blakesley and D. Neher, Relationship between energetic disorder and open-circuit voltage in bulk heterojunction organic solar cells, Phys. Rev. B **84**, 075210 (2011).

[9] W. Gong, M. A. Faist, N. J. Ekins-Daukes, Z. Xu, D. D. C. Bradley, J. Nelson, and T. Kirchartz, Influence of energetic disorder on electroluminescence emission in polymer:fullerene solar cells, Phys. Rev. B **86**, 024201 (2012).

[10] S. D. Collins, C. M. Proctor, N. A. Ran, and T.-Q. Nguyen, Understanding open-circuit voltage loss through the density of states in organic bulk heterojunction solar cells, Adv. Energy Mater. **6**, 1501721 (2016).

[11] G. Garcia-Belmonte and J. Bisquert, Open-circuit voltage limit caused by recombination through tail states in bulk heterojunction polymer-fullerene solar cells, Appl. Phys. Lett. **96**, 113301 (2010).

[12] R. A. Street, Localized state distribution and its effect on recombination in organic solar cells, Phys. Rev. B **84**, 075208 (2011).

[13] N. R. Monohan, K. W. Williams, B. Kumar, C. Nuckolls, and X.-Y. Zhu, Direct observation of entropy-driven electron-hole pair separation at an organic semiconductor interface, Phys. Rev. Lett. **114**, 247003 (2015).

[14] S. N. Hood and I. Kassal, Entropy and disorder enable charge separation in organic solar cells, J. Phys. Chem. Lett. 7, 4495 (2016).

[15] L. J. A. Koster, E. C. P. Smits, V. D. Mihailetchi, and P. W. M. Blom, Device model for the operation of polymer/fullerene bulk heterojunction solar cells, Phys. Rev. B **72**, 085205 (2005).

[16] N. C. Giebink, G. P. Wiederrecht, M. R. Wasielewski, and S. R. Forrest, Ideal diode equation for organic heterojunctions. I. Derivation and application, Phys. Rev. B **82**, 155305 (2010).

[17] A. Melianas, V. Pranculis, A. Devižis, V. Gulbinas, O. Inganäs, and M. Kemerink, Dispersion-dominated photocurrent in polymer:fullerene solar cells, Adv. Funct. Mater. **24**, 4507 (2014).

[18] A. Melianas, F. Etzold, T. J. Savenije, F. Laquai, O. Inganäs, and M. Kemerink, Photo-generated carriers lose energy during extraction from polymer-fullerene solar cells, Nat. Comm. **6**, 8778 (2015).

[19] A. Melianas, V. Pranculis, Y. Xia, N. Felekidis, O. Inganäs, V. Gulbinas, and M. Kemerink, Photogenerated carrier mobility significantly exceeds injected carrier mobility in organic solar cells, Adv. Energy Mater. **7**, 1602143 (2017).

[20] V. M. Le Corre, A. R. Chatri, N. Y. Doumon, and L. J. A. Koster, Charge carrier extraction in organic solar cells governed by steady-state mobilities, Adv. Energy Mater. **7**, 1701138 (2017).

[21] R. Pandey, A. A. Gunawan, K. A. Mkhoyan, R. J. Holmes, Efficient organic photovoltaic cells based on nanocrystalline mixtures of boron subphthalocyanine chloride and C60, Adv. Funct. Mater. **22**, 617 (2012).

[22] A. E. Jailaubekov, A. P. Willard, J. R. Tritsch, W.-L. Chan, N. Sai, R. Gearba, L. G. Kaake, K. J. Williams, K. Leung, P. J. Rossky, and Y-Y. Zhu, Hot charge-transfer excitons set the time limit for charge separation at donor/acceptor interfaces in organic photovoltaics, Nat. Mater. **12**, 66 (2013).

[23] J. Orenstein and M. A. Kastner, Thermalization and recombination in amorphous semiconductors, Solid State Commun. **40**, 85 (1981).

[24] A. Hofacker, J. O. Oelerich, A. V. Nenashev, F. Gebhard, and S. D. Baranovskii, Theory to carrier recombination in organic disordered semiconductors, J. Appl. Phys. **115**, 223713 (2014).

[25] A. Hofacker and D. Neher, Dispersive and steady-state recombination in organic disordered semiconductors, Phys. Rev. B **96**, 245204 (2017).

[26] P. B. Deotare, W. Chang, E. Hontz, D. N. Congreve, L. Shi, P. D. Reusswig, B. Modtland, M. E. Bahlke, C. K. Lee, A. P. Willard, V. Bulović, T. Van Voorhis, and M. A. Baldo, Nanoscale transport of charge-transfer states in organic donor–acceptor blends, Nat. Mater. **14**, 1130 (2015).

[27] D. Jarzab, F. Cordella, J. Gao, M. Scharber, H.-J. Egelhaaf, and M. A. Loi, Low-temperature behaviour of charge transfer excitons in narrow-bandgap polymer-based bulk heterojunctions, Adv. Energy Mater. **1**, 604 (2011).

[28] K. Vandewal, J. Widmer, T. Heumueller, C. J. Brabec, M. D. McGehee, K. Leo, M. Riede, and A. Salleo, Increased open-circuit voltage of organic solar cells by reduced donor-acceptor interface area, Adv. Mater. **26**, 3839 (2014).

[29] See Supplemental Material at URL for a comparison of pure material and CT PL, analysis of the impact of temperature-dependent absorption on the CT PL log ratio, reference GaAs PL and log ratios, CT PL from 1:2 and 4:1 SubPc:C_{60} blends, power-dependence of CT PL spectra, and a summary of non-thermal behavior from additional OPV blend systems.

[30] J. Nelson, Diffusion-limited recombination in polymer-fullerene blends and its influence on photocurrent collection, Phys. Rev. B **67**, 155209 (2003).

[31] A. Maurano, R. Hamilton, C. G. Shuttle, A. M. Ballantyne, J. Nelson, C. O'Regan, W. Zhang, I. McCulloch, H. Azimi, M. Morana, C. J. Brabec, and J. R. Durrant, Recombination dynamics as a key determinant of open circuit voltage in organic bulk heterojunction solar cells: A comparison of four different donor polymers, Adv. Mater. **22**, 4987 (2010).

[32] C. G. Shuttle, B. O'Regan, A. M. Ballantyne, J. Nelson, D. D. C. Bradley, and J. R. Durrant, Bimolecular recombination losses in polythiophene: Fullerene solar cells, Phys. Rev. B 78, 113201 (2008).

[33] K. Vandewal, K. Tvingstedt, A. Gadisa, O. Inganäs, and J. V. Manca, Relating the open-circuit voltage to interface molecular properties of donor:acceptor bulk heterojunction solar cells, Phys. Rev. B **81**, 125204 (2010).

[34] P. Würfel, The chemical potential of radiation, J. Phys. C: Solid State Phys. **15**, 3967 (1982).

[35] K. Schick, E. Daub, S. Finkbeiner, and P. Würfel, Verification of a generalized Planck law for luminescence radiation from silicon solar cells, Appl. Phys. A **54**, 109 (1992).

[36] T. Trupke, P. Würfel, I. Uhlendorf, and I. Lauermann, Electroluminescence of the dye-sensitized solar cell, J. Phys. Chem. B **103**, 1905 (1999).

[37] J. K. Katahara and H. W. Hillhouse, Quasi-Fermi level splitting and sub-bandgap absorptivity from semiconductor photoluminescence, J. Appl. Phys. **116**, 173504 (2014).

[38] U. Rau, Reciprocity relation between photovoltaic quantum efficiency and electroluminescent emission of solar cells, Phys. Rev. B **76**, 085303 (2007).

[39] K. Vandewal, K. Tvingstedt, A. Gadisa, O. Inganäs, and J. V. Manca, On the origin of the open-circuit voltage of polymer–fullerene solar cells, Nat. Mater. **8**, 904 (2009).

[40] T. Kirchartz, J. Nelson, and U. Rau, Reciprocity between charge injection and extraction and its influence on the interpretation of electroluminescence spectra in organic solar cells, Phys. Rev. Appl. **5**, 054003 (2016).

[41] B. Feuerbacher and P. Würfel, Verification of a generalised Planck law by investigation of the emission from GaAs luminescent diodes, J. Phys. Condens. Matter **2**, 3803 (1990).

[42] K. Tvingstedt, K. Vandewal, F. Zhang, and O. Inganäs, On the dissociation efficiency of charge transfer excitons and frenkel excitons in organic solar cells: A luminescence quenching study, J. Phys. Chem. C **114**, 21824 (2010).

[43] L. J. A. Koster, V. D. Mihailetchi, R. Ramaker, and P. W. M. Blom, Light intensity dependence of open-circuit voltage of polymer:fullerene solar cells, Appl. Phys. Lett. **86**, 123509 (2005).

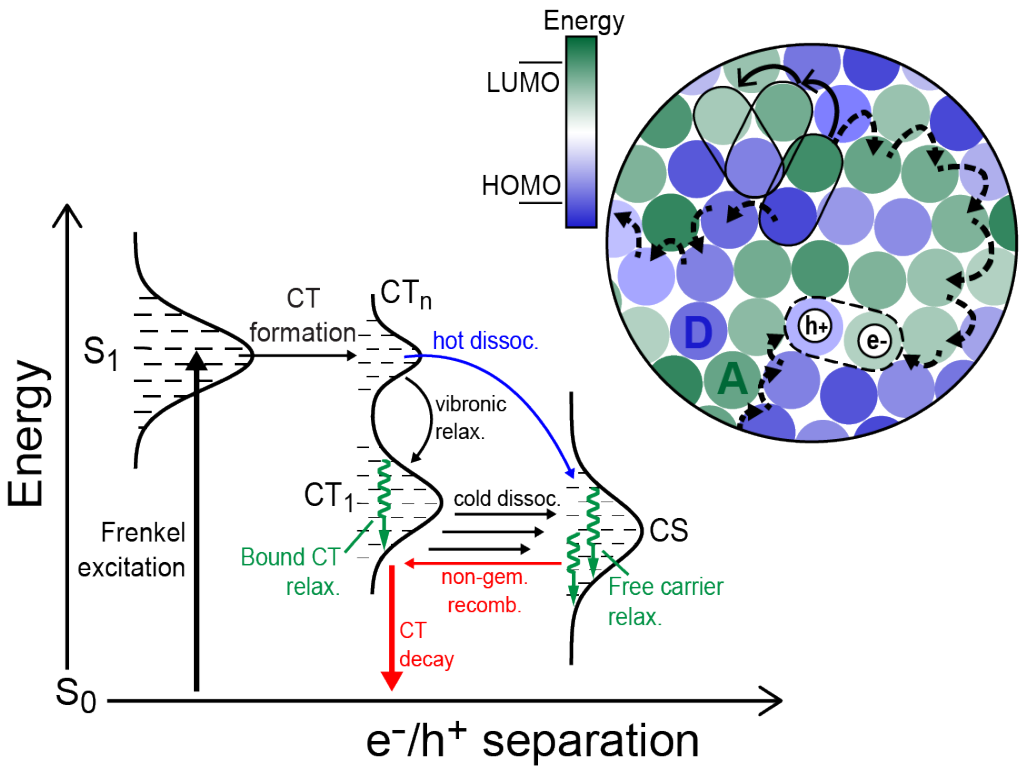

FIG. 1. Schematic showing charge separation, relaxation, and recombination pathways within the disorder-broadened CT and free carrier density of states distributions in a typical OPV DA blend. Once formed, CT states may relax geminately through correlated motion of the electron and hole toward lower energy sites (Process 1, shown by the solid arrows in the inset) or they may dissociate into free carriers that relax independently and recombine to form non-geminate CT states (Process 2, shown by the dashed arrows).

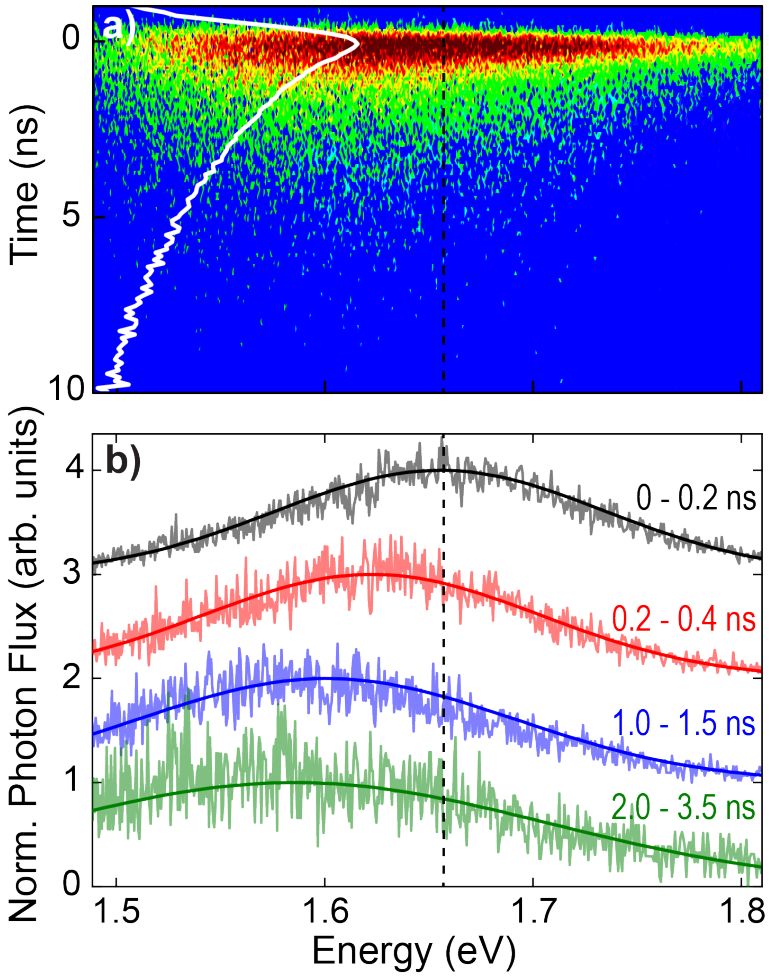

FIG. 2. (a) Streak camera image showing the CT PL decay of a 1:1 blend SubPc:C_{60} film. The dashed line shows the peak PL energy at the onset of emission. (b) Photoluminescence spectra integrated over different time intervals in the streak image, showing a redshift of the emission peak within the first few nanoseconds of the decay. The solid lines are Gaussian fits to the data and the vertical dashed line denotes the PL peak energy immediately following the excitation pulse.

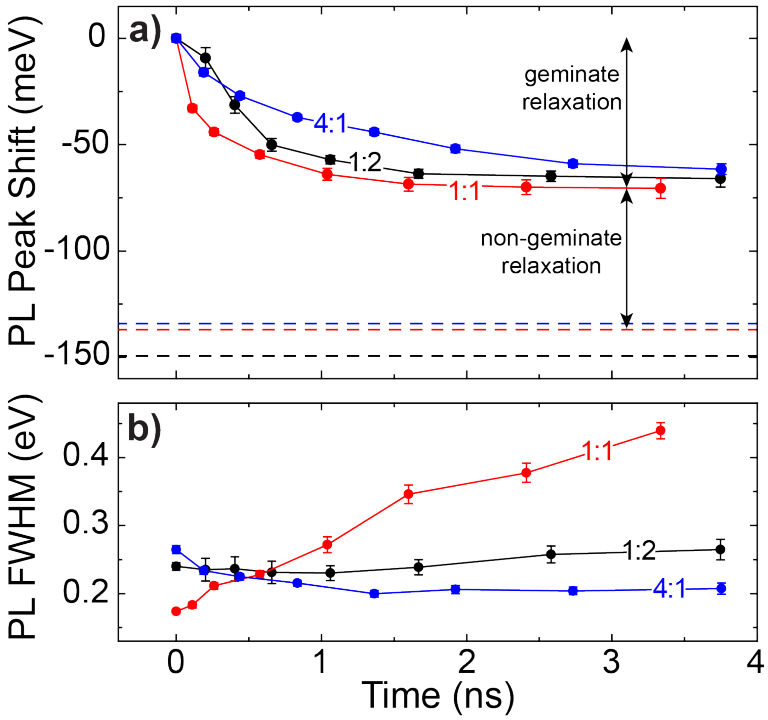

FIG. 3. (a) Redshift of the CT PL emission peak as a function of time for different SubPc:C_{60} blend ratios. The corresponding color dashed lines indicate the full shift to steady-state. (b) Full-width half-maximum broadening of the same CT PL spectra over time. The peak energy and broadening are extracted from Gaussian fits to the emission spectra as shown in Fig. 2(b).

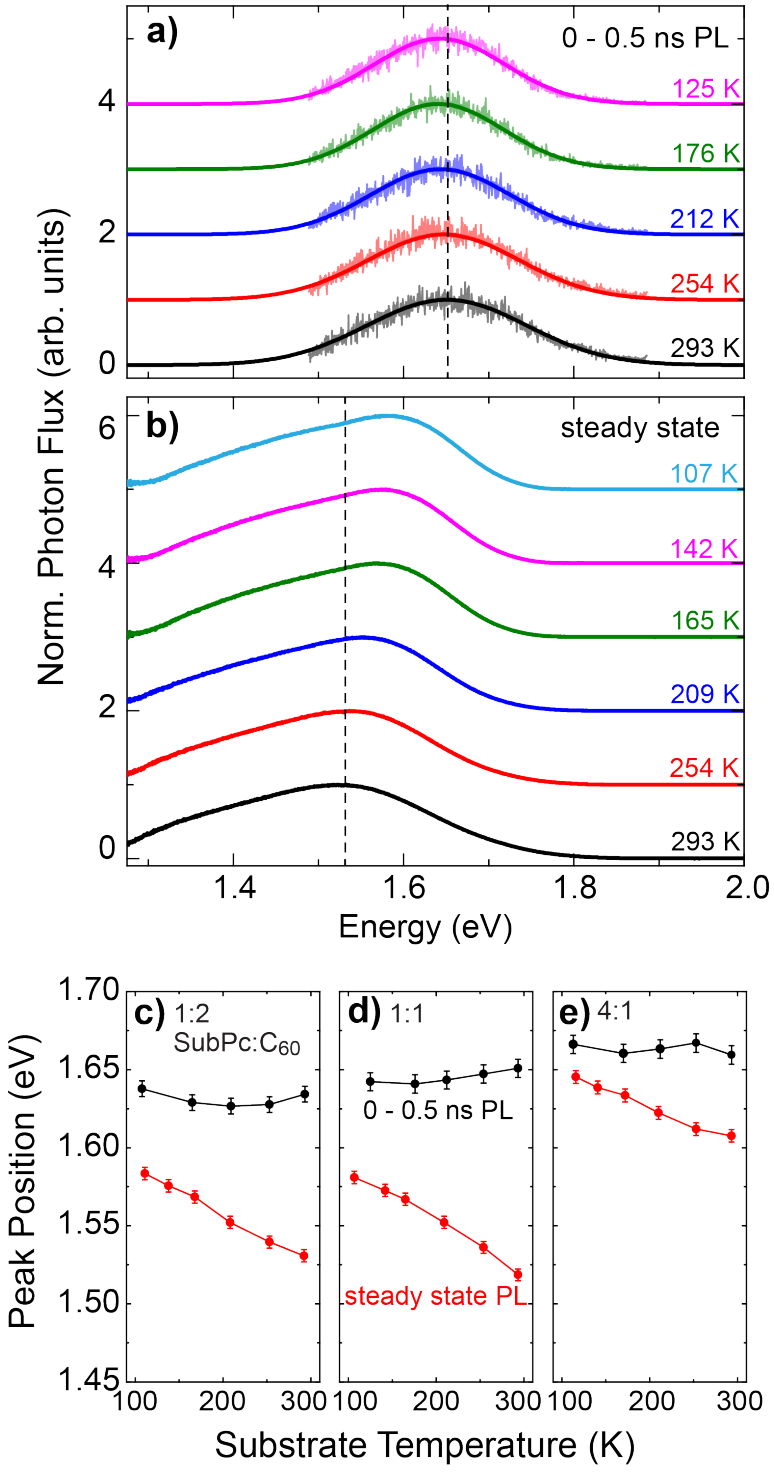

FIG. 4. Early time CT PL spectra collected from a 1:1 SubPc:C_{60} blend within the first 0.5 ns following excitation (a) and at steady state under continuous-wave illumination (b) for different sample temperatures. Dashed black lines in (a) and (b) denote the emission peak energy of each

data set at room temperature. (c)-(e) Summary of the variation in early time and steady-state CT PL peak energies as a function of temperature for each SubPc:C_{60} blend (full spectra provided in the Supplemental Material [29]).

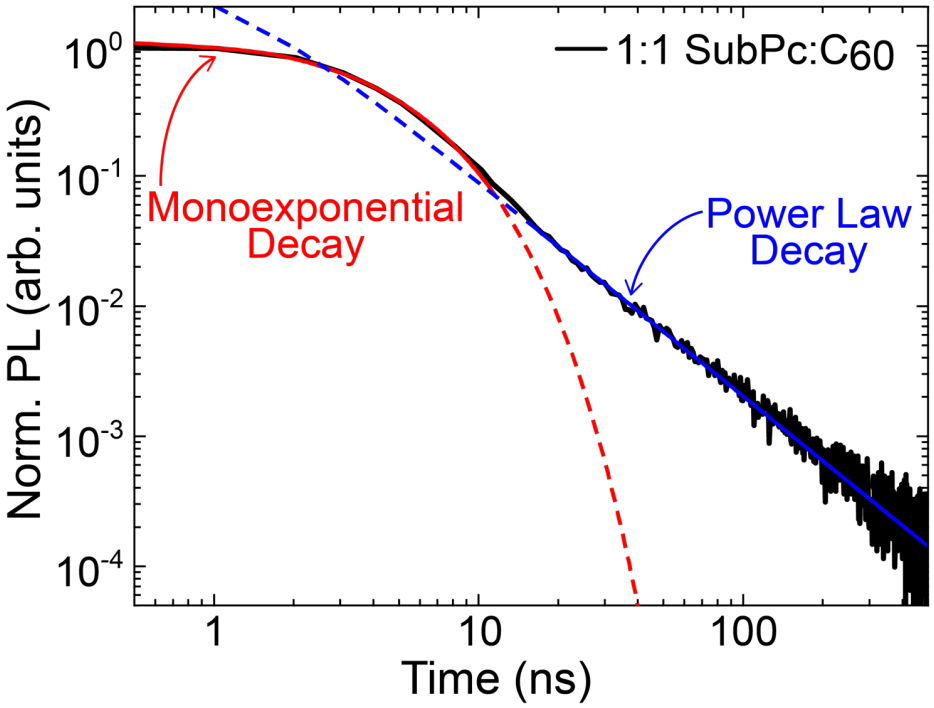

FIG. 5. CT PL decay collected from a 1:1 SubPc:C_{60} film at a substrate temperature of 102 K (black line). The data exhibit two clear regimes: monoexponential decay ($\propto e^{-t/\tau}$, with $\tau = 3.9$ ns) at early times < 10 ns that is consistent with geminate CT recombination, and a power law decay ($\propto t^{-\alpha}$, with $\alpha = 1.6$) at longer times that is characteristic of non-geminate recombination in an energetically-disordered system [30-32]. The red and blue lines overlaid on the data show these individual functional dependences.

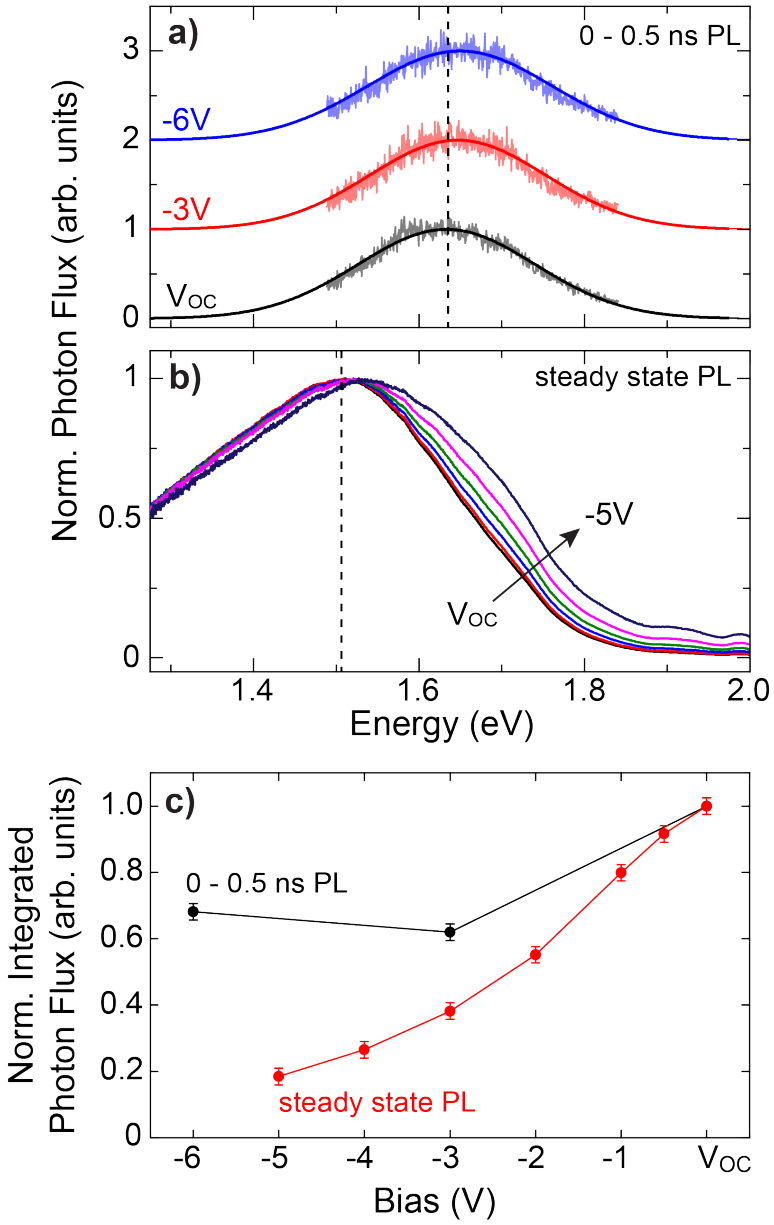

FIG. 6. (a) Early time CT PL spectra collected within the first 0.5 ns following excitation from a 1:1 SubPc:C_{60} blend solar cell at different reverse bias values. (b) Steady-state emission from the same device collected under continuous-wave illumination over the same bias range. The vertical dashed line in each panel marks the peak of the emission spectrum at open circuit. (c) Integrated intensity of the early time and steady-state CT PL spectra in (a) and (b) as a function of reverse bias, normalized to that at open circuit.

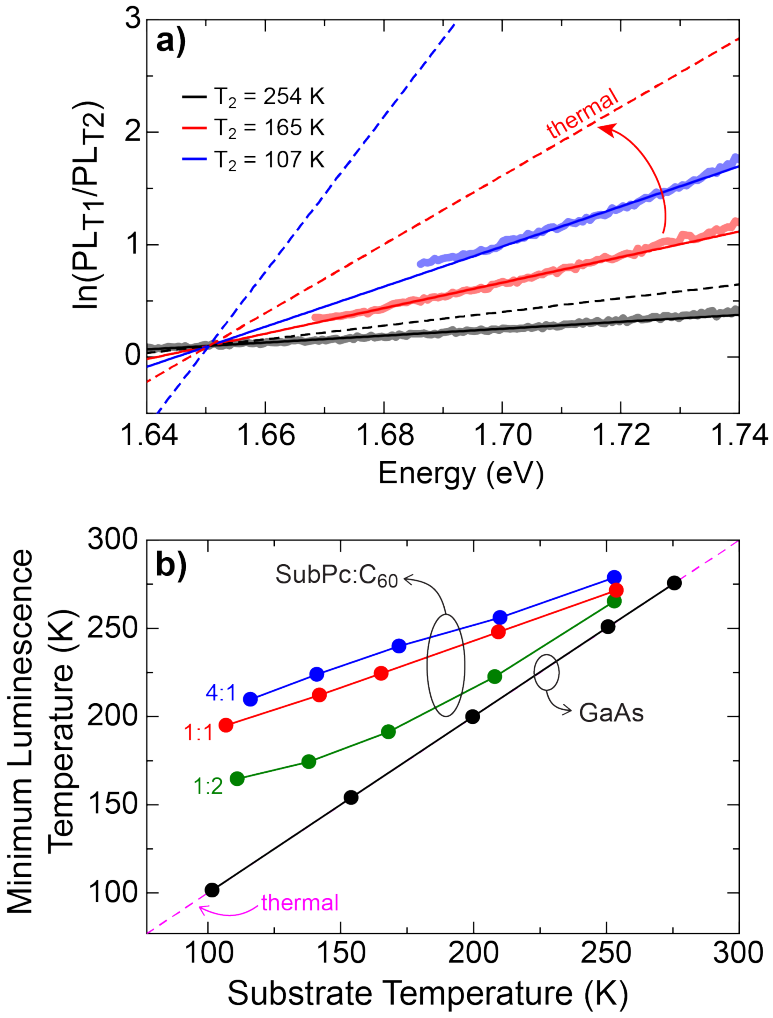

FIG. 7. (a) Log ratios of the temperature-dependent CT PL spectra shown in Fig. 4(b), using the room temperature spectrum (T_1 = 293 K) as the reference. Light solid lines show the experimental log ratios, dark solid lines show linear fits to the data, and the dashed lines denote the linear slopes that would occur in each case if the luminescence temperature corresponded to the actual sample temperature. (b) Summary of the effective luminescent temperatures extracted from the log PL ratios of each SubPc:C_{60} blend as well as a GaAs wafer for reference. The pink dashed line marks thermal luminescence with a temperature equal to that of the substrate.

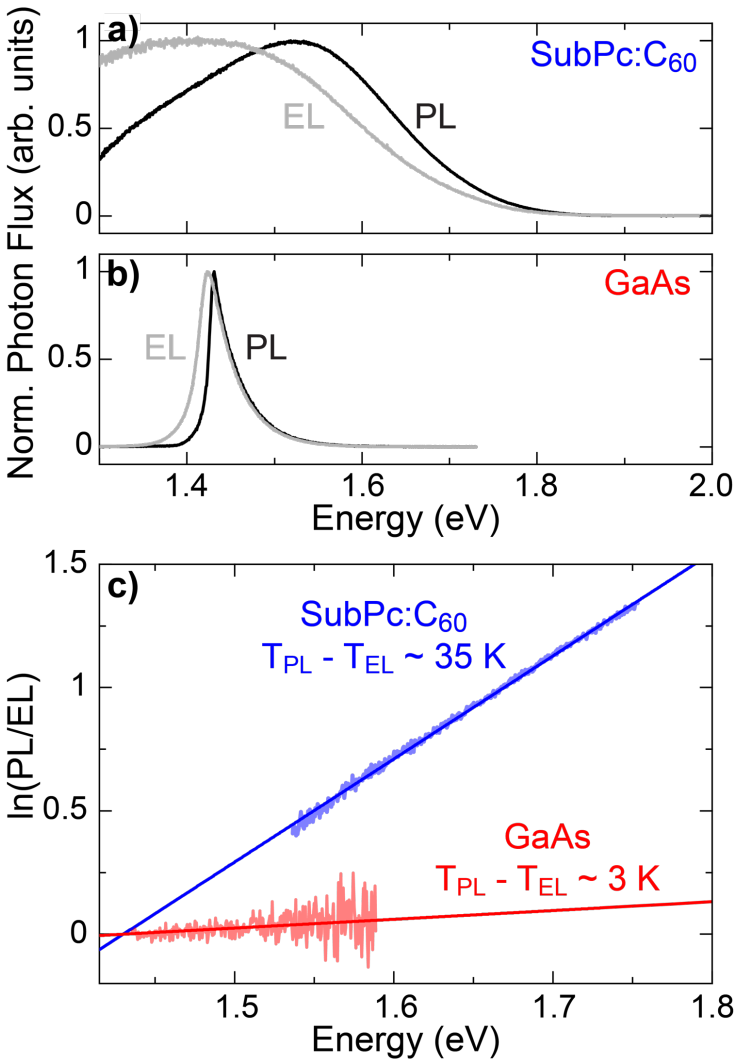

FIG. 8. (a) Steady-state EL and PL spectra collected from a 1:1 SubPc:C_{60} solar cell at room temperature. (b) The same data measured from a GaAs solar cell (EL) and wafer (PL). The EL drive current density for the OPV and GaAs cell was 300 mA/cm^2 and 20 mA/cm^2, respectively. (c) PL-to-EL log ratios of each device. Assuming the EL to be at room temperature in each case, the SubPc:C_{60} slope indicates an effective PL temperature elevated by ~35 K, whereas the EL and PL temperatures of GaAs differ only negligibly.